A&A, 709, A136 (2026)
https://doi.org/10.1051/0004-6361/202658878

Astronomy & Astrophysics

The effect of recurrent fluorescence on the survival probability of hot octasulfur cations

P. Ferrari[1,⋆], M. H. Stockett[2], P. Martini[2], J. E. Navarro Navarrete[2], H. Cederquist[2], L. B. F. M. Waters[1,3], H. T. Schmidt[2], H. Zettergren[2], and J. M. Bakker[1,4]

[1] HFML-FELIX, Nijmegen, The Netherlands
[2] Department of Physics, Stockholm University, Stockholm, Sweden
[3] Department of Astrophysics, IMAPP, Radboud University, Nijmegen, The Netherlands
[4] Institute for Molecules and Materials, Radboud University, Nijmegen, The Netherlands

Received 7 January 2026 / Accepted 4 April 2026

ABSTRACT

Context. Sulfur allotropes are proposed as a contributor to the missing atomic sulfur in the interstellar medium, in particular octasulfur, regarded as the most stable sulfur allotrope. Models of sulfur chemical pathways in the ISM strongly rely on the stability of octasulfur.
Aims. We investigate the de-excitation dynamics of hot S_8^+ ions in the gas-phase, addressing experimentally the competition between fragmentation, vibrational cooling, and recurrent fluorescence. By combining the experiments with calculations of rate coefficients, we elucidate the survival probability of octasulfur, placing constraints on the interstellar environments where the allotrope can be detected.
Methods. Experiments are performed at the cryogenic ion beam storage ring DESIREE at Stockholm University. Thermally hot S_8^+ ions are injected into the storage ring, where the time-dependent fragmentation yield is measured. In addition, using inputs from quantum chemical calculations, the energy-dependent rate coefficients of fragmentation, vibrational cooling, and recurrent fluorescence are modeled. The dynamics of the excited-state populations in S_8^+ is studied based on a master equation formalism, providing the survival probability of the ions as a function of internal energy. The analysis is also extended to the neutral S_8 allotrope.
Results. We observe that radiative cooling is efficient on a time scale of 95 ms, corresponding to internal energies in the range of 1.1–1.4 eV. Experimentally, two fragmentation channels are observed, following the pathways $S_8^+ \rightarrow S_5^+ + S_3$ and $S_8^+ \rightarrow S_6^+ + S_2$, in agreement with previous studies. From the computations, these channels have dissociation energies of 1.8 and 1.4 eV, respectively. The modeled rate coefficients predict very slow vibrational cooling, whereas those of recurrent fluorescence are consistent with the experiment. Recurrent fluorescence is expected to proceed from an electronic state at 0.76 eV, computed by time-dependent density functional theory. The analysis reveals a survival probability of less than 1% at internal energies higher than 1.70 eV. In contrast, calculations predict that recurrent fluorescence is not a competitive cooling channel in neutral S_8, which promptly fragments above 1.4 eV.
Conclusions. Recurrent fluorescence is predicted to be a competitive cooling channel for S_8^+, providing a stabilizing pathway for ions in hot environments. Based on simulated survival probabilities, an upper limit of 1100 K is found for the temperature of interstellar environments where S_8^+ could be detected. However, recurrent fluorescence is not effective for neutral S_8, which will fragment already at internal energies close to its dissociation limit.

Key words. astrochemistry – molecular data – radiation mechanisms: general – ISM: abundances – ISM: molecules

1. Introduction

Understanding the chemical pathways of sulfur in the interstellar medium (ISM) remains a puzzle (Mifsud et al. 2021). Whereas in diffuse low-density interstellar environments the abundance of atomic sulfur roughly corresponds to the known cosmic value (Goicoechea et al. 2006; Fuente et al. 2024), in dense molecular clouds, star-forming regions, and planet-forming disks there is a major depletion of gas phase atomic sulfur, by up to two orders of magnitude (Le Gal et al. 2021; Laas & Caselli 2019). Gas-phase sulfur-bearing molecules, such as HCS, OCS, and SO_2 have been detected (Agúndez et al. 2018; Van Gelder et al. 2024), but at concentrations far too low to account for the missing sulfur. Sulfur can also be present in volatile ices, salts, or in the more refractory species FeS. Recently, OCS (tentatively detected using Akari; Aikawa et al. 2012) and potentially SO_2 ice were detected in lines of sight towards cold molecular clouds using the *James Webb* Space Telescope. However, H_2S ice, expected to be abundant, was not detected (McClure et al. 2023). Moreover, evidence has been presented that ammonium salts may contain a significant amount of sulfur in the form of NH_4SH, possibly accounting for 17–18 percent of the sulfur budget (Slavicinska et al. 2025). Refractory FeS is abundant in solar system interplanetary dust (IDP) grains of cometary origin, suggesting that a significant but difficult to quantify fraction of sulfur may be in the form of FeS in planet-forming disks (Keller & Messenger 2011).

Another class of molecules proposed as a possible sink for the missing sulfur is composed by sulfur allotropes (Jiménez-Escobar & Caro 2011; Carrascosa et al. 2024) formed in interstellar ices, of which S_8 stands out as a prominent candidate. Indeed, density functional theory (DFT) calculations predict octasulfur to be the most stable S_N allotrope (Fedyaeva et al. 2023). Sulfur allotropes were identified in trace abundances in the coma of comet 67 P/Churyumov-Gerasimenko12, in particular S_2, S_3, and S_4 (Calmonte et al. 2016), while S_8 was detected in Ryugu

⋆ Corresponding author: piero.ferrariramirez@ru.nl

samples (Aponte et al. 2023). Astrochemical models describing the chemical pathways of sulfur-bearing molecules have been proposed, showing that among the different S_N allotropes, S_8 is the most abundant (Shingledecker et al. 2020; Taillard et al. 2025), given its higher fragmentation energy. However, these models lack fundamental experimental information about absorption cross sections, dissociation energies, fragmentation channels, and de-excitation mechanisms, in general. Recently, infrared absorption cross sections of S_8, S_4^+, and S_4^- were quantified, based on a combination of infrared spectroscopy and DFT calculations (Ferrari et al. 2024). In addition, the work revealed a relatively low dissociation energy for S_8 (1.4 eV), as well as for its cationic counterpart, S_8^+, with a competition of two fragmentation channels: the formation of pentamers and hexamers. These results highlight a more complex chemical network of sulfur allotropes than anticipated, in which the formation and destruction of octasulfur can occur in energetic environments. An open question remains about the survival probability of octasulfur in these interstellar environments, which can guide a targeted search in the ISM via astronomical observations, as well as providing key pieces of information to improve astrochemical models. Given that not only neutrals but also charged molecules have been found in space (McGuire 2022), such information is relevant for both S_8 and S_8^+, which may behave differently.

In isolated conditions, where excess energy cannot be dissipated through an external heat bath, the survival probability of a thermally hot molecule is determined by three processes: fragmentation, electron emission, and radiative cooling. Here, a system is considered hot if it has a total excitation energy, equilibrated throughout its degrees of freedom, higher than its lowest dissociation energy (Hansen 2013). Under thermally hot conditions, one of the possible cooling channels typically dominates, but depending on the internal energy and molecule-specific parameters, competition can occur. Radiative cooling, which can stabilize a molecule against fragmentation if active, can proceed through two distinct mechanisms, namely direct vibrational cooling (VC) or recurrent fluorescence (RF; Zhu et al. 2022; Ito et al. 2014; Andersen et al. 2001). The latter process is also called Poincaré fluorescence, as initially suggested in the pioneering work of Léger and coworkers (Léger et al. 1988). In conventional VC, excess energy is dissipated through the emission of infrared photons through a cascade of vibrational transitions (Hansen et al. 2023). Given that in VC multiple low-energy photons are emitted through transitions with low oscillator strength, for a fixed molecular size, cooling is slow and only competitive with dissociation or electron emission at internal energies close to the threshold energies for these processes (Stockett et al. 2020). Instead, in RF, photons are emitted via electronic transitions, therefore having larger oscillator strengths and requiring only a single photon to quench any further fragmentation (Kono et al. 2015). However, for RF to be competitive to fragmentation, a molecule must possess electronic states low enough in energy to allow inverse internal conversion (IIC) to take place (Kaw et al. 2024).

To date, RF has been indirectly shown to be a competitive cooling channel in a variety of carbon-bearing molecules, including polycyclic aromatic hydrocarbons (PAHs; Martin et al. 2013; Lee et al. 2023), fullerenes (Hansen & Campbell 1996; Sundén et al. 2009; Navarrete et al. 2025), and small carbon clusters (Iida et al. 2022; Chandrasekaran et al. 2014), as well as different metal clusters (Peeters et al. 2021; Ferrari et al. 2018; Hansen et al. 2017a). To date, direct detection of RF photons has only been achieved for four systems: C_4^- (Yoshida et al. 2017), C_6^- (Ebara et al. 2016), $C_{10}H_6^+$ (Saito et al. 2020), and $C_{14}H_{10}^+$ (Kusuda et al. 2024). Interestingly, detailed experiments on cationic 1-cyanonaphthalene have shown an enhanced survival probability for these molecules when RF is an effective cooling channel (Stockett et al. 2023). Indeed, small PAHs have been detected in the ISM (Wenzel et al. 2024; Cernicharo et al. 2026; Cabezas et al. 2025), in environments conventionally assumed to be too harsh for such small species to survive (Andrews et al. 2015). Instead, observations show abundances of orders of magnitude higher than predicted by astrochemical models, for example, cyanonaphthalene and cyanopyrene (McGuire et al. 2021; Wenzel et al. 2024), suggesting that stabilization by RF is an important factor for evaluating astrophysical survival.

Here, using an electrostatic storage ring setup, we show that radiative cooling is an active cooling channel in S_8^+ cations. Employing inputs from quantum chemical calculations, the rate coefficients of fragmentation, VC, and RF are calculated as a function of the internal energy, revealing that radiative cooling proceeds via RF in this all-sulfur molecule. Based on the simulated rates, the energy-dependent survival probability of S_8^+ is calculated, highlighting the effect of RF on the survival of S_8^+ at high internal energies. The analysis is also extended to neutral S_8, in which RF is not an active process. This allows us to place limits on the interstellar environments in which octasulfur could be detected.

2. Methods

2.1. Experimental details

The experiments were performed at the DESIREE facility (Double ElectroStatic Ion Ring ExpEriment) of Stockholm University (Thomas et al. 2011; Schmidt et al. 2013; Schmidt 2021). DESIREE consists of two coupled electrostatic ion-beam storage rings, but in these experiments only one ring was used, as shown schematically in Fig. 1. The circumference of the ion orbit in this ring is about 8.7 m. The cryogenic ring is cooled to ≈13 K, which results in low residual gas densities and consequently very long storage times (Gatchell et al. 2014; Bäckström et al. 2015; Gatchell et al. 2014). The α-sulfur powder was sublimed in a resistively heated oven coupled to an electron cyclotron resonance (ECR) ion source, using He as the carrier gas. The S_8^+ cations generated (m/z = 256) were extracted from the source and accelerated to 34 keV, followed by mass selection using a bending magnet before injection into the storage ring.

The ionization process leaves the ions with internal energies sufficiently high to induce fragmentation, a process that occurs continuously along their travel in the ring. Neutrals formed by fragmentation in the observation arm of the ring, depicted at the bottom in Fig. 1, were counted by a position-sensitive imaging detector (neutral detector), placed after a deflection unit in the ring. If multiple fragmentation channels exist in S_8^+, this detector counts the total fragmentation yield. In addition, a second position-sensitive detector was mounted next to the stored beam after deflection (fragment detector), as depicted in the figure. This detector collects charged fragmentation products formed by fragmentation, which can be identified through m/z-specific deflection angles. An example of a measurement with the fragment detector is shown in the top-left corner of Fig. 1, revealing the competing generation of S_5^+ and S_6^+ ions – in both cases in correlation with a neutral reaction product. This implies the fragmentation channels $S_8^+ \rightarrow S_5^+ + S_3$ and $S_8^+ \rightarrow S_6^+ + S_2$. The position of the fragment detector was optimized for the detection of S_5^+. Charged fragments, S_5^+ and S_6^+, and neutral fragments were

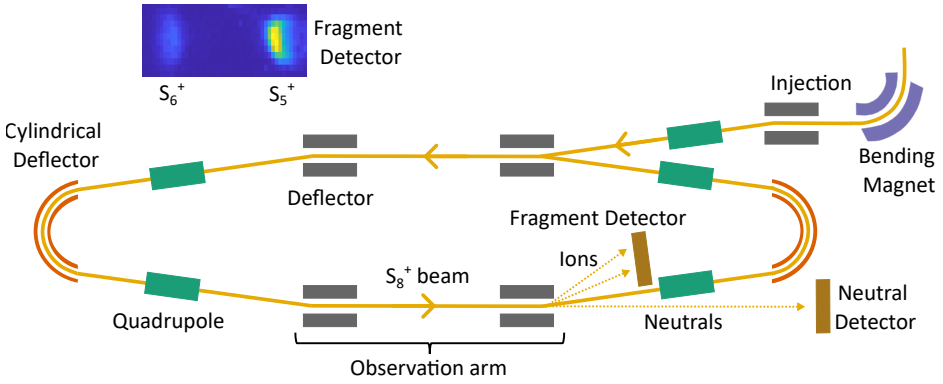

Fig. 1. Schematic view of the storage ring DESIREE. A 34 keV beam of S_8^+ ions is mass selected by a bending magnet and is injected into the cold ring. The circulation direction of the ions is depicted by arrows. A detector for neutrals formed upon fragmentation is placed after the straight section opposite to injection. In addition, a second detector is placed on the side of the stored S_8^+ beam, after a 10° deflection, to measure the charged species created by fragmentation. Both detectors are position-sensitive. In the top-left corner, an image of the fragment detector is shown, depicting ions corresponding to S_5^+ and S_6^+.

continuously recorded for 1.2 seconds, after which the remaining current was measured with a Faraday cup. This measurement cycle was repeated a large number of times.

2.2. Quantum chemical calculations and modeling

To model the rate coefficients of fragmentation k_D, vibrational cooling k_{VC}, and recurrent fluorescence k_{RF} as a function of internal energy E, inputs from DFT calculations are required. For this purpose, DFT calculations were performed using the ORCA 6.0.1 software package (Neese 2022, 2023). The B3LYP exchange-correlation functional was employed (Becke 1992), together with the Def2-TZVPP basis set (Becke 1992), including dispersion corrections via the D3BJ method (Grimme et al. 2010). This combination was recently used to compute the vibrational spectra of S_8, S_4^+, and S_4^-, showing a very close agreement with measurements of their gas-phase infrared spectra (Ferrari et al. 2024). Calculations were performed with the non-default "verytight" convergence criterium for the SCF procedure and geometry optimization, as previously done. Based on the measured fragmentation channels of S_8^+, the calculation of k_D, k_{VC}, and k_{RF} requires the harmonic vibrational frequencies of the allotropes S_8^+, S_6^+, S_5^+, S_3, and S_2, as discussed below. The starting geometries for optimization of the allotropes were extracted from a previous work (Jin et al. 2015). No scaling factor was applied to the computed frequencies (Ferrari et al. 2024). Moreover, for the modeling of k_D, the dissociation energies of the pathways $S_8^+ \rightarrow S_6^+ + S_2$ and $S_8^+ \rightarrow S_5^+ + S_3$ were required. These were taken from previous work, reported to be 1.4 and 1.8 eV for the emission of dimers and trimers, respectively (Ferrari et al. 2024). Finally, crucial factors in the calculation of k_{RF} are the optically active electronic transitions of S_8^+, which we computed using time-dependent DFT (TD-DFT) at the same theoretical level as the vibrational calculations.

The fragmentation rate coefficient of S_8^+ dissociating via the channel $S_8^+ \rightarrow S_{8-i}^+ + S_i$ is expressed as (Hansen 2013)

$$k_D(E)^i = \omega_i \frac{\rho_{8-i}(E - D_i)}{\rho_8(E)}. \tag{1}$$

Here, ρ_8 and ρ_{8-i} are the densities of the vibrational levels of S_8^+ and S_{8-i}^+, respectively, which were calculated by the Beyer-Swinehart algorithm (Beyer & Swinehart 1973). In addition, D_i is the dissociation energy of the channel and ω_i the corresponding frequency factor. The latter was estimated based on sulfur vapor pressures, as previously discussed (Veldeman et al. 2008; Hansen et al. 2014; Chen et al. 2019).

For k_{VC}, the simple harmonic cascade (SHC) approximation was used, which leads to the expression in Eq. (2) (Chandrasekaran et al. 2014). Here, ν_s and A_s^{IR} are the frequency and Einstein A-coefficient of vibrational mode s, respectively, and n is the vibrational quantum number

$$k_{VC}(E) = \sum_s k_s^{VC} = \sum_s A_s^{IR} \sum_{n=1}^{n \le E/h\nu_s} \frac{\rho_8(E - nh\nu_s)}{\rho_8(E)}. \tag{2}$$

The recurrent fluorescence rate coefficient is (Ferrari et al. 2019)

$$k_{RF}(E) = \sum_e k_e^{RF} = \sum_e A_e^{RF} \frac{\rho_8(E - h\nu_e)}{\rho_8(E)}, \tag{3}$$

where A_e^{RF} is the Einstein A-coefficient of the electric transition at energy $h\nu_e$, while e runs over the electronic transitions of S_8^+. The first ten electronic transitions are considered, although numerically only the first state contributes to RF (see details later).

Finally, the dynamics of the population of excited states was modeled using a master equation formalism (Lee et al. 2023), describing the survival probability of the excited S_8^+. For this, the population distribution of hot S_8^+ molecules, $g(E, t)$, was propagated through Eq. (4), which describes the change in g in energy E due to fragmentation and radiation

$$\begin{aligned} \frac{\mathrm{d}}{\mathrm{d}t} g(E,t) = &- \sum_c k_D^c(E) g(E,t) \\ &+ \sum_s \left[k_s^{VC}(E + h\nu_s) g(E + h\nu_s, t) - k_s^{VC}(E) g(E,t) \right] \\ &+ \sum_e \left[k_e^{RF}(E + h\nu_e) g(E + h\nu_e, t) - k_e(E)^{RF} g(E,t) \right]. \end{aligned} \tag{4}$$

The three terms describe the change in population at energy E due to fragmentation, vibrational cooling, and recurrent fluorescence, respectively. In Eq. (4), c runs over the two possible

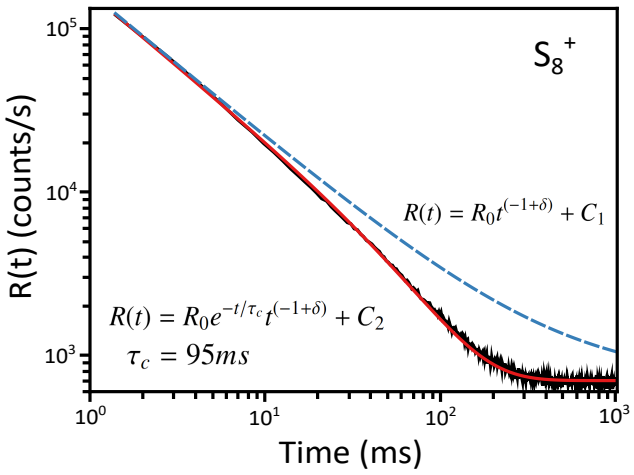

Fig. 2. Time-dependent neutral yield of S_8^+ ions. A quenched power law (Eq. (6)) is fitted to the experimental data, shown in the continuous red line. In addition, a simple power law (Eq. (5)) is included in the dashed blue line for comparison, showing the presence of radiative cooling.

dissociation channels of S_8^+. We note that in this model approach, internal vibrational redistribution (IVR) is assumed to be efficient at all times (or internal energies).

3. Results and discussion

3.1. Fragmentation channels

The use of the fragment detector, as shown in Fig. 1, allowed us to obtain information about the fragmentation pathways of vibrationally hot S_8^+ ions. As already mentioned, only the formation of two charged products, S_5^+ and S_6^+, was observed, implying that two fragmentation pathways compete: $S_8^+ \rightarrow S_5^+ + S_3$ and $S_8^+ \rightarrow S_6^+ + S_2$. This observation agrees with previous experiments in which collision-induced dissociation (CID) was used to infer the fragmentation channels of S_8^+ and the competition between the formation of S_5^+ and S_6^+ (Ferrari et al. 2024). This reinforces that atom-by-atom evaporation is not an energetically favorable dissociation pathway for S_8^+, which instead emits neutral dimers and trimers. Previous work on neutral S_8 has shown the same fragmentation pathways, i.e., $S_8 \rightarrow S_5 + S_3$ and $S_8 \rightarrow S_6 + S_2$ (Ferrari et al. 2024), albeit using a third excitation mechanism to induce fragmentation, infrared multiple photon excitation. Hence, it seems clear that irrespective of the excitation mechanism and its charge state, octasulfur fragments by emitting neutral S_2 and S_3 units, a behavior currently not included in astrochemical models of sulfur allotropes (Laas & Caselli 2019; Shingledecker et al. 2020). DFT calculations show that among the possible octasulfur fragmentation channels, the emissions of neutral S_2 and S_3 fragments have the lowest threshold energies.

3.2. Fragmentation time-dependence

The neutral yield (count rate) $R(t)$ of S_8^+ ions, accounting for S_2 and S_3 fragments, is measured using the neutral detector as a function of storage time, as shown by the black trace in Fig. 2. At early times, when the S_8^+ ensemble is hot, a high neutral yield is recorded, implying a high fragmentation rate. In time, however, the state population of S_8^+ shifts to lower energies, leading to a much lower fragmentation rate. This is clearly observed in the figure, with a decrease in the detected neutral yield up to ≈300 ms. From this time on, fragmentation occurs only at a very low rate, most likely dominated by collisions with the residual gas in the storage ring.

As shown by many studies of storage rings and ion traps, given the broad energy distribution of the ensemble, the overall decay dynamics follows a power law in time, with an exponent shown to be close to −1. However, this is under the assumption that only fragmentation is responsible for the cooling of the stored ensemble of ions (Hansen et al. 2001, 2017b). This is known as the $1/t$ decay law, which is a consequence of the fact that the ensemble decays at different rates simultaneously for different internal ion energies, if the internal energy distribution is broad (Andersen et al. 2003). Hence, when only fragmentation occurs in the ensemble of hot S_8^+ ions, the measured neutral yield $R(t)$ follows Eq. (5), with R_0, δ, and C_1 constants

$$R(t) = R_0 t^{(-1+\delta)} + C_1. \tag{5}$$

Deviations from the $1/t$ law, i.e., $\delta \neq 0$ have been tentatively assigned to effects of heat capacity, competing channels, and the shape of the internal energy distribution (Hansen 2021). An attempt to fit Eq. (5) to the data in Fig. 2 (dashed blue line) reveals a good agreement at short times, but clearly cannot grasp the full time-dependence of $R(t)$, especially not for longer storage times. Hence, the power law decay works only at higher internal energies. Instead, if radiative cooling competes with fragmentation, the power law is exponentially quenched (Ferrari et al. 2019)

$$R(t) = R_0 e^{-t/\tau_c} t^{(-1+\delta)} + C_2, \tag{6}$$

with τ_c the critical radiative cooling time, where the dissociation and radiative rate coefficients are roughly equal. As presented in Fig. 2, a fit of Eq. (6) reproduces the time-dependence of the observed signal well, yielding a value of $\tau_c = 95 \pm 1$ ms. From the fit, we further extract $R_0 = (1127 \pm 1) \cdot 10^3$ and $\delta = 0.106 \pm 0.001$, and a background of $4 \cdot 10^3$. Hence, the analysis shows that radiation is an effective cooling channel for S_8^+ ions. However, knowledge of τ_c alone cannot distinguish between vibrational cooling and recurrent fluorescence, for which modeling of the different rate coefficients is necessary.

3.3. Rates of fragmentation, vibrational cooling, and recurrent fluorescence

Following the procedure discussed in the Methods section, and using Eq. (1), the total fragmentation rate coefficient of S_8^+ is modeled as a function of internal energy. The result is presented in Fig. 3a as a solid green curve. Given the activated nature of fragmentation, the process stops below the lowest dissociation energy of S_8^+, computed as 1.4 eV using DFT (Ferrari et al. 2024). The region in between the horizontal dashed lines denotes the dynamical range to which the experiment is sensitive. Above the upper line, fragmentation will occur faster than the time it takes S_8^+ to cover half a turn in the ring, whereas the rates below the lower line correspond to time scales longer than the total storage time in the ring in the present experiment (1.2 s).

In addition, the figure shows the rate of vibrational cooling (short-dashed red line). For this, Eq. (2) is used, which needs as input the vibrational frequencies of S_8^+. We relied on DFT calculations for the frequencies, using a recently applied method to successfully compute the infrared spectra of S_8, S_4^+ and S_4^- (Ferrari et al. 2024). The infrared spectrum presented in that reference reveals only a few infrared-active modes, all of low intensity due to the relatively high symmetry of S_8^+.

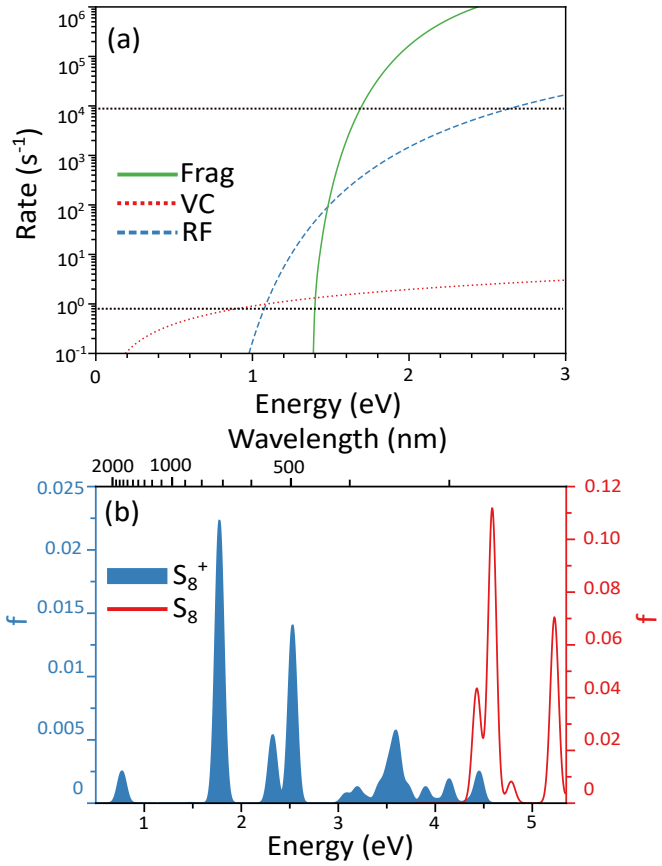

Fig. 3. (a) Modeled rates of fragmentation (solid green line), vibrational cooling (dotted red line) and recurrent fluorescence (dashed blue line). The region in between the horizontal dotted lines highlights the dynamical range covered experimentally. (b) TD-DFT-computed optical absorption spectrum of S_8^+ (filled blue) and S_8 (red). The y-axis represents oscillator strength (f). A top axis in wavelength is included.

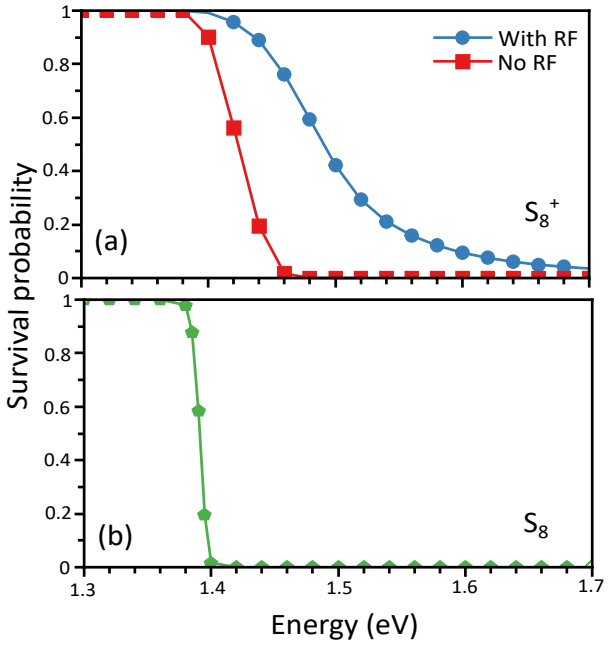

Fig. 4. (a) Survival probability of S_8^+ as a function of initial internal energy (blue circles). The situation in which RF is excluded is presented in red squares. (b) Survival probability of neutral S_8.

As a consequence, the VC rate is low, barely reaching values within the experimentally sensitive region and would give a critical time of 770 ms, much longer than the measured value of $\tau_c = 95 \pm 1$ ms. Hence, another process should be invoked to explain the experimental results.

Finally, Fig. 3a presents the modeled rate of recurrent fluorescence (dashed blue line). In this case, the analysis requires the optically active electronic transitions of S_8^+, which we computed using TD-DFT. To assess the reproducibility of such calculations, we also computed the optical spectrum of S_8, which can be compared with measurements performed in methanol solution (Steudel et al. 1988). The experimental data show broad absorption features at roughly 270 (4.59) and 235 (5.28) nm (eV), in close agreement with predicted optical transitions at 270 (4.59) and 237 (5.23) nm (eV). The calculated absorption spectra of S_8^+ and S_8 are shown in Fig. 3b. Given the closed-shell electronic configuration of neutral S_8, electronic transitions are only found at high energies, above 4.42 eV. Instead, for the open-shell S_8^+, a low-lying electronic transition is predicted at 0.76 eV, which is the main source of RF. When comparing the rates of fragmentation and RF, a much better correspondence is found with the experiment than in the case of VC. For RF, a critical rate of 80 s^{-1} is predicted, slightly different from the experimental value of $\tau_c = 95 \pm 1$ s^{-1} but on the same order of magnitude. Considering a typical uncertainty of ±0.2 eV for the computation of transition energies with TD-DFT using hybrid functionals (Laurent & Jacquemin 2013), the modeled RF rates are reasonably close to the experimental value.

3.4. Survival probability

Astrochemical models accounting for sulfur allotropes assume that S_8 is the end of the reaction chain (Shingledecker et al. 2020), given the predicted higher stability of octasulfur with respect to other allotropes. However, recent DFT calculations of dissociation energies (Ferrari et al. 2024) showed much lower values than other species present in the ISM, such as PAHs and C_{60}. This raises the question of the survival probability of octasulfur in energetic interstellar environments, which ultimately determines where octasulfur could be detected in space.

To address this, we used the formalism of Eq. (4) to model the survival probability of S_8^+ as a function of internal energy. Starting from an initial delta function distribution centered at energy E_0, the rates of fragmentation, VC, and RF (Fig. 3a) were employed to track the distribution as a function of time. Equation (4) is numerically solved in steps of 0.05 µs, for a total time of 1 s. The survival probability is defined as the ratio of the integrated initial and final population distribution. The result for S_8^+ is presented in Fig. 4a, which also depicts the situation when RF is excluded from the analysis. As seen, without RF, the probability rapidly falls to zero at internal energies above 1.4 eV. Instead, RF helps stabilize S_8^+, which now has a survival probability of 50% at an energy of 1.49 eV. With RF, there is still a survival probability of 1% at an internal energy of 1.7 eV. Hence, RF provides a stabilizing pathway, but the effect is not dramatic. Assuming a heat capacity of $(3N - 6)k_B$, this means a temperature of 1100 K as the limit for the environments in which S_8^+ could be detected.

Although the experiments presented here are performed only on the cationic S_8^+, the analysis of the rate coefficients can be extended to the neutral S_8. As shown in Fig. 3b, S_8 only has electronic transitions at energies above 4 eV, and therefore RF is

not a possible cooling channel, leaving only fragmentation and VC. In this case, the survival probability rapidly falls to zero above 1.4 eV, making the temperature constraint lower, implying that above 900 K S_8 will promptly fragment.

4. Conclusions

Experiments on hot S_8^+ ions were performed in the cryogenic ion-beam storage ring DESIREE, showing quenching of fragmentation by radiative cooling on a critical time scale of 95 ms. Fragmentation was seen to proceed via two competitive channels: $S_8^+ \rightarrow S_5^+ + S_3$ and $S_8^+ \rightarrow S_6^+ + S_2$, in agreement with previous collision-induced dissociation experiments (Ferrari et al. 2024). Interestingly, these channels are the same as for neutral S_8. Using inputs from quantum chemical calculations, the rate coefficients of fragmentation, vibrational cooling, and recurrent fluorescence were modeled, showing good agreement with the experiment. The analysis revealed that radiative cooling in S_8^+ proceeds via RF from a low-lying electronic transition at 0.76 eV. Nevertheless, the stabilization provided by RF is not drastic and at internal energies greater than 1.7 eV there is a survival probability of less than 1% for S_8^+, which has a lowest dissociation energy of 1.4 eV. The analysis was extended to neutral S_8, in which RF is not a possible cooling mechanism due to the lack of low-lying electronically excited states. For S_8, destruction already occurs immediately from the dissociation-energy limit of 1.4 eV.

Acknowledgements. We acknowledge the DESIREE infrastructure for provisioning of facilities and experimental support, and thank the operators and technical staff for their invaluable assistance. The DESIREE infrastructure receives funding from the Swedish Research Council under the grant numbers 2021-00155 and 2023-00170. H.Z., H.C., and H.T.S. thank the Swedish Research Council for individual project grants (with Contracts No.2025-05087, No.2023-03833, and No.2022-02822). Furthermore, H.T.S, H.C., and H.Z. acknowledge the project grant "Making and Breaking of Molecular Bonds" funded by the Knut and Alice Wallenberg Foundation under contract 2024.0134. This article is based upon work from COST Action CA21126 - Carbon molecular nanostructures in space (NanoSpace), supported by COST (European Cooperation in Science and Technology). We further acknowledge the Dutch Research Council (NWO) for support through computational resources (grant 2024.009).

References

Agúndez, M., Marcelino, N., Cernicharo, J., & Tafalla, M. 2018, A&A, 611, L1
Aikawa, Y., Kamuro, D., Sakon, I., et al. 2012, A&A, 538, A57
Andersen, J. U., Gottrup, C., Hansen, K., Hvelplund, P., & Larsson, M. 2001, Eur. Phys. J. D, 17, 189
Andersen, J. U., Bonderup, E., Hansen, K., et al. 2003, Eur. Phys. J. D., 24, 191
Andrews, H., Boersma, C., Werner, M., et al. 2015, ApJ, 807, 99
Aponte, J. C., Dworkin, J. P., Glavin, D. P., et al. 2023, EPS, 75, 28
Bäckström, E., Hanstorp, D., Hole, O. M., et al. 2015, Phys. Rev. Lett., 114, 143003
Becke, A. D. 1992, J. Chem. Phys., 96, 2155
Beyer, T., & Swinehart, D. 1973, CACM, 16, 379
Cabezas, C., Agúndez, M., Pérez, C., et al. 2025, A&A, 701, L8
Calmonte, U., Altwegg, K., Balsiger, H., et al. 2016, MNRAS, 462, S253
Carrascosa, H., Muñoz Caro, G., Martín-Doménech, R., et al. 2024, MNRAS, 533, 967
Cernicharo, J., Tercero, B., Marcelino, N., et al. 2026, A&A, 705, L7
Chandrasekaran, V., Kafle, B., Prabhakaran, A., et al. 2014, J. Phys. Chem. Lett., 5, 4078
Chen, F.-Q., Kono, N., Suzuki, R., et al. 2019, Phys. Chem. Chem. Phys., 21, 1587
Ebara, Y., Furukawa, T., Matsumoto, J., et al. 2016, Phys. Rev. Lett., 117, 133004
Fedyaeva, M., Lepeshkin, S., & Oganov, A. R. 2023, Phys. Chem. Chem. Phys., 25, 9294
Ferrari, P., Vanbuel, J., Hansen, K., et al. 2018, Phys. Rev. A, 98, 012501
Ferrari, P., Janssens, E., Lievens, P., & Hansen, K. 2019, Int. Rev. Phys. Chem., 38, 405
Ferrari, P., Berden, G., Redlich, B., Waters, L. B., & Bakker, J. M. 2024, Nat. Commun., 15, 5928
Fuente, A., Roueff, E., Le Petit, F., et al. 2024, A&A, 687, A87
Gatchell, M., Schmidt, H. T., Thomas, R. D., et al. 2014 , J. Phys. Conf. Ser. 488, 012040
Goicoechea, J., Pety, J., Gerin, M., et al. 2006, A&A, 456, 565
Grimme, S., Antony, J., Ehrlich, S., & Krieg, H. 2010, J. Chem. Phys., 132, 154104
Hansen, K. 2013, Statistical Physics of Nanoparticles in the Gas Phase (Berlin: Springer), 73
Hansen, K. 2021, Mass Spectrom. Rev., 40, 725
Hansen, K., & Campbell, E. 1996, J. Chem. Phys., 104, 5012
Hansen, K., Andersen, J. U., Hvelplund, P., et al. 2001, Phys. Rev. Lett., 87, 123401
Hansen, K., Li, Y., Kaydashev, V., & Janssens, E. 2014, J. Chem. Phys., 141, 024302
Hansen, K., Ferrari, P., Janssens, E., & Lievens, P. 2017a, Phys. Rev. A, 96, 022511
Hansen, K., Stockett, M. H., Kaminska, M., et al. 2017b, Phys. Rev. A, 95, 022511
Hansen, K., Licht, O., Kurbanov, A., & Toker, Y. 2023, J. Phys. Chem. A, 127, 2889
Iida, S., Hu, W., Zhang, R., et al. 2022, MNRAS, 514, 844
Ito, G., Furukawa, T., Tanuma, H., et al. 2014, Phys. Rev. Lett., 112, 183001
Jiménez-Escobar, A., & Caro, G. M. 2011, A&A, 536, A91
Jin, Y., Maroulis, G., Kuang, X., et al. 2015, Phys. Chem. Chem. Phys., 17, 13590
Kaw, K. A., Louwerse, R. J., Bakker, J. M., et al. 2024, Commun. Chem., 7, 124
Keller, L. P., & Messenger, S. 2011, Geochim. Cosmochim. Acta, 75, 5336
Kono, N., Furukawa, T., Tanuma, H., et al. 2015, Phys. Chem. Chem. Phys., 17, 24732
Kusuda, J., Fukuzaki, R., Majima, T., Tsuchida, H., & Saito, M. 2024, Nucl. Instrum. Methods Phys. Res. B, 553, 165387
Laas, J. C., & Caselli, P. 2019, A&A, 624, A108
Laurent, A. D., & Jacquemin, D. 2013, Int. J. Quantum Chem., 113, 2019
Le Gal, R., Öberg, K. I., Teague, R., et al. 2021, ApJS, 257, 12
Lee, J. W., Stockett, M. H., Ashworth, E. K., et al. 2023, J. Chem. Phys., 158
Léger, A., Boissel, P., & d'Hendecourt, L. 1988, Phys. Rev. Lett., 60, 921
Martin, S., Bernard, J., Brédy, R., et al. 2013, Phys. Rev. Lett., 110, 063003
McClure, M. K., Rocha, W., Pontoppidan, K., et al. 2023, Nat. Astron., 7, 431
McGuire, B. A. 2022, ApJS, 259, 30
McGuire, B. A., Loomis, R. A., Burkhardt, A. M., et al. 2021, Science, 371, 1265
Mifsud, D. V., Kaňuchová, Z., Herczku, P., et al. 2021, Space Sci. Rev., 217, 14
Navarrete, J. N., Martini, P., Rosén, S., et al. 2025, Phys. Rev. Lett., 135, 213001
Neese, F. 2022, Wiley Interdiscip. Rev. Comput. Mol. Sci., 12, e1606
Neese, F. 2023, J. Comput. Chem., 44, 381
Peeters, K., Janssens, E., Hansen, K., Lievens, P., & Ferrari, P. 2021, Phys. Rev. Research., 3, 033225
Saito, M., Kubota, H., Yamasa, K., et al. 2020, Phys. Rev. A, 102, 012820
Schmidt, H. T. 2021, in ECLA (Berlin: Springer), 183
Schmidt, H. T., Thomas, R. D., Gatchell, M., et al. 2013, Rev. Sci. Instrum., 84, 055115
Shingledecker, C. N., Lamberts, T., Laas, J. C., et al. 2020, ApJ, 888, 52
Slavicinska, K., Boogert, A., van Dishoeck, E., et al. 2025, A&A, 693, A146
Steudel, R., Jensen, D., Göbel, P., & Hugo, P. 1988, Ber. Bunsenges. Phys. Chem., 92, 118
Stockett, M. H., Bull, J. N., Buntine, J. T., et al. 2020, Eur. Phys. J. D, 74, 150
Stockett, M. H., Bull, J. N., Cederquist, H., et al. 2023, Nat. Commun., 14, 395
Sundén, A., Goto, M., Matsumoto, J., et al. 2009, Phys. Rev. Lett., 103, 143001
Taillard, A., Martín-Doménech, R., Carrascosa, H., et al. 2025, A&A, 694, A263
Thomas, R. D., Schmidt, H. T., Andler, G., et al. 2011, Rev. Sci. Instrum., 82, 065112
Van Gelder, M., Ressler, M., Van Dishoeck, E., et al. 2024, A&A, 682, A78
Veldeman, N., Janssens, E., Hansen, K., et al. 2008, Faraday Discuss., 138, 147
Wenzel, G., Cooke, I. R., Changala, P. B., et al. 2024, Science, 386, 810
Yoshida, M., Furukawa, T., Matsumoto, J., et al. 2017, J. Phys. Conf. Ser., 875, 102016
Zhu, B., Bull, J. N., Ji, M., Zettergren, H., & Stockett, M. H. 2022, J. Chem. Phys., 157, 044303